Sahel Rainfall–Tropical Easterly Jet Relationship on Synoptic to Intraseasonal Time Scales

ALEXANDER LEMBURG

International Max Planck Research School on Earth System Modelling, Max Planck Institute for Meteorology, Hamburg, Germany

JÜRGEN BADER

Max Planck Institute for Meteorology, Hamburg, Germany, and Uni Climate, Uni Research, and the Bjerknes Centre for Climate Research, Bergen, Norway

MARTIN CLAUSSEN

Max Planck Institute for Meteorology, and Meteorologisches Institut, Centrum für Erdsystemforschung und Nachhaltigkeit, Universität Hamburg, Hamburg, Germany

ABSTRACT

The tropical easterly jet (TEJ) is a characteristic upper-level feature of the West African monsoon (WAM) circulation. Moreover, the TEJ over West Africa is significantly correlated with summer Sahel rainfall on interannual and decadal time scales. In contrast, the relationship between Sahel rainfall and the regional TEJ on synoptic to intraseasonal time scales is unclear. Therefore, this relationship is investigated by means of multiple statistical analyses using temporally highly resolved measurement and reanalysis data. It is shown that average correlations between convective activity and regional TEJ intensity remain below 0.3 for all synoptic to intraseasonal time scales. Especially on the synoptic time scale, the TEJ significantly lags anomalies in convective activity by one or two days, which indicates that convection anomalies are more likely to drive changes in the regional TEJ than vice versa. To further shed light on the role of the TEJ for rainfall over West Africa, a previously proposed effect of TEJ-induced upper-level divergence on the development of mesoscale convective systems (MCSs) is examined more closely. An analysis of nearly 300 Sahelian MCSs shows that their initiation is generally not associated with significant TEJ anomalies or jet-induced upper-level divergence. Furthermore, no statistically significant evidence is found that preexisting TEJ-related upper-level divergence anomalies affect intensity, size, and lifetime of MCSs. A limiting factor of this study is the focus on TEJ-induced upper-level divergence. Therefore, a possible effect of the TEJ on Sahel rainfall via other mechanisms cannot be ruled out and should be subject to future studies.

1. Introduction

Rainfall in sub-Saharan West Africa is inextricably linked to the West African monsoon (WAM), which is characterized by a pronounced seasonal wind shift initiated by thermodynamic contrasts between land and ocean. A prominent feature of the summertime WAM circulation is the tropical easterly jet (TEJ), an upper-tropospheric (100–200 hPa) easterly current between 5° and 20°N, first described by Rao (1952) and Koteswaram (1958). The TEJ originates in the South Asian monsoon system over the Bay of Bengal, extends westward to Africa and decays over the tropical Atlantic. Observations, reanalyses and model simulations have shown that anomalously wet years in the Sahel are often characterized by a regionally stronger TEJ compared to its
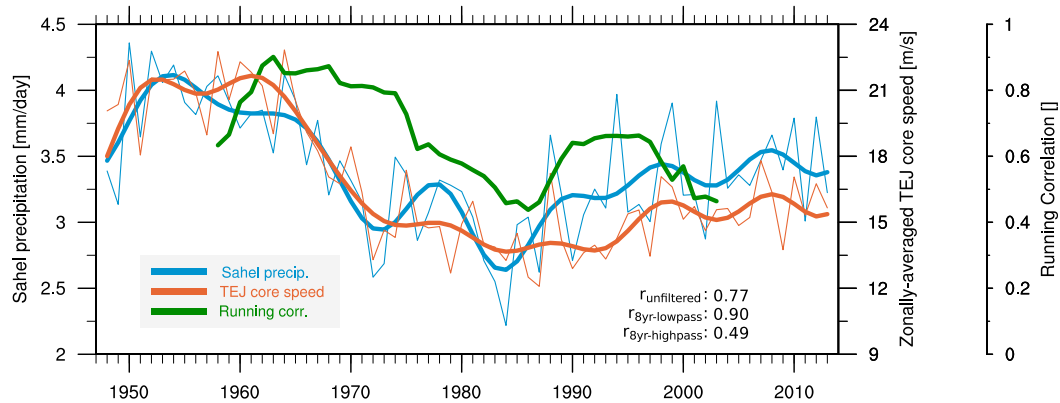
FIG. 1. Time series from 1948 to 2013 of JJAS Sahel precipitation (from CRU 3.2 data spatially averaged over 10°W–10°E and 10°–20°N) and JJAS 200 hPa TEJ core speed. (For a representative core speed measure that is insensitive to latitude changes, the average JJAS TEJ core speed was calculated from daily NCEP–NCAR reanalysis fields of 200 hPa zonal wind data as follows: within a domain between 10°W and 10°E and 5°S and 25°N, the daily maximum of easterly 200 hPa zonal wind speed is found for each longitudinal strip of grid points. The found maximum speeds of each longitude are then averaged over the whole domain to obtain an average speed of the TEJ core.) Thin, light lines depict the unfiltered yearly means. Thick lines show the 10-yr low-pass-filtered time series. The green line depicts the 21-yr running correlation.

summer [June–September (JJAS)] climatology whereas dry years exhibit a weaker TEJ over West Africa (e.g., Grist and Nicholson 2001; Sylla et al. 2010).

Figure 1 shows that not only decadal trends (thicker lines) are very similar, but even on a year-to-year basis changes in rainfall often coincide with changes in TEJ intensity. Years with higher Sahel precipitation are on average accompanied by a regionally enhanced TEJ south of the main rainband (Fig. 2). This distinct regional maximum might be mainly considered as the time-integrated response of the regional upper-level circulation to the positive diabatic heating anomaly of a wetter than normal monsoon season. Nonetheless, it would probably be mistaken to view the TEJ exclusively as a passive by-product of the WAM circulation because the TEJ and WAM rainfall might substantially interact with each other. Moreover, Nicholson (2009) suggested that "the link between the TEJ and rainfall is a causal one with the strong TEJ enhancing rainfall by enhancing upper-level divergence." Redelsperger et al. (2002) highlighted that the dynamic configuration between convection and the TEJ over West Africa exhibits similarities with that observed for midlatitude jets and stressed the uncertainty with regard to the cause and effect relationship. Assessing a number of synoptic cases, Besson and Lemaître (2014) found that upper-level divergence in the entrance region of regional TEJ maxima (jet streaks) might play an important role by promoting development of mesoscale convective systems (MCSs).

However, previous studies cannot fully prove or explain substantial interaction between the TEJ and Sahel rainfall. Nicholson (2013) only provides a qualitative

picture by suggesting two mechanisms (divergence, wave disturbances) by which the TEJ might influence rainfall. The findings of Besson and Lemaître (2014) might not be generally valid as they are only based on
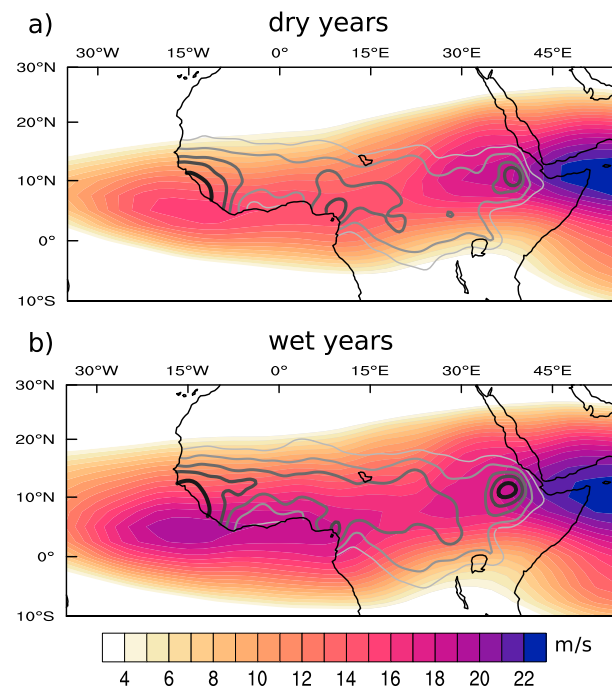

FIG. 2. Composite comparison of August easterly 200 hPa zonal wind from NCEP–NCAR for interannually measured (a) dry and (b) wet Sahel years. For the composite, the eight driest and wettest years of the 15-yr high-pass-filtered CRU precipitation dataset since 1948 were chosen. The gray contour lines depict CRU August precipitation in form of the 2, 4, 7, 10, and 15 mm day^{-1} isohyet.

one in-depth and 16 brief synoptic case studies. Therefore, further research is needed to gain a more comprehensive view of the possible role of the TEJ in modulating WAM rainfall.

In the first part, this study quantifies the covariability and the lead–lag relationship between the TEJ and Sahel rainfall over a range of synoptic to intraseasonal time scales. For this, spectral analysis, lead–lag correlations and regression analysis are applied to a 32-yr-long record of daily outgoing longwave radiation as proxy for rainfall and daily output from multiple reanalyses. The second part of this study challenges the ideas of Besson and Lemaître (2014), who suggested that TEJ streaks aid MCS development, mainly by inducing significant upper-level divergence. Theoretical considerations, which follow in the next section, render a pivotal role of the TEJ on MCS initiation via upper-level divergence unlikely. A secondary order effect of TEJ-related divergence on convective initiation cannot be ruled out, though, and a possible impact on MCS organization is still an open question. We therefore extend the work of Besson and Lemaître (2014) and provide a more complete statistical investigation of upper-level winds before the initiation of Sahelian MCSs, also testing whether changes in MCS lifetime, size or intensity are associated with TEJ-induced divergence. In contrast to Besson and Lemaître (2014), our analysis is not limited to a few individual MCS events, but involves roughly 300 MCS initiation cases in the period 2007–15, allowing us to assess statistical significance.

2. Theoretical background

The subseasonal variability of WAM precipitation can be broken up into three time scales: 2–8 day (referred to as synoptic-scale variability hereafter), 10–25-day, and 30–90-day variability. Synoptic-scale variability dominates on smaller regional scales ($\sim$1000 km) and is strongly linked to westward propagating wave disturbances, so-called African easterly waves (AEWs), with typical wavelengths between 2000 and 5000 km and periods of mostly 2–7 days (Carlson 1969; Burpee 1972; Kiladis et al. 2006; Mekonnen et al. 2006). At larger spatial scales ($\gg$1000 km), synoptic-scale variability is not as important and rainfall variability is increasingly confined to time scales longer than 10 days. On the 10–25-day time scale two dominant modes of variability exist: the quasi-biweekly zonal dipole mode (QBZD) (Mounier et al. 2008) which only affects the southern parts of the Sahel and the so-called Sahel mode (Sultan et al. 2003; Janicot et al. 2010). The QBDZ is characterized by a quasi-stationary zonal dipole of convection and a corresponding Walker-type circulation between

the Guinean coast and the western part of the equatorial Atlantic which changes sign about every 7 days. The Sahel mode is associated with a first northward and then westward propagating signal of enhanced convective activity starting over central Africa, traveling through the Sahel region and dissipating over the equatorial Atlantic. Variability on the lower-frequency band (30–90 days) is mainly associated with the Madden–Julian oscillation (MJO; Maloney and Shaman 2008; Alaka and Maloney 2012). In contrast to WAM precipitation, subseasonal variability of the West African TEJ has been much less studied and it is not clear whether it is linked to any of the abovementioned modes. The first part of this study aims to close this gap.

From a more phenomenological than statistical point of view, Sahel rainfall is mainly linked to the number of mesoscale convective systems (MCSs; Lebel et al. 2003; Lebel and Ali 2009). Of particular importance are large and well-organized MCSs which move westward with speeds between 10 and 15 m s^{-1} and often persist for more than 24 h. Although such MCSs represent only 12% of all convective systems in the Sahel, they are responsible for up to 90% of all rainfall over that region (Mathon et al. 2002).

For any kind of deep, moist convection to occur, three necessary ingredients have to be in place at the same time (Doswell et al. 1996): Besides the presence of 1) sufficiently moist air and 2) a conditionally unstable stratification, 3) a lifting mechanism is needed to lift a parcel to its level of free convection (LFC). In the Sahel, convective inhibition is often high and therefore vigorous lift is required to raise a parcel to its LFC. Sufficient lift can be produced by orography, cold pools or mesoscale circulations arising from surface inhomogeneities (Lafore et al. 2017). While such mesoscale scale processes are pivotal for the initiation of deep convection, synoptic-scale atmospheric dynamics might also play an important role in the formation and in particular organization of deep, moist convection. Over 60% of organized squall lines in summer are associated with AEWs (Fink and Reiner 2003) suggesting that synoptic-scale dynamics might be a crucial factor for well-organized Sahelian MCSs. Whereas convective clouds can be found in each sector of AEWs, most organized convective systems tend to occur at or ahead of the trough (Diedhiou et al. 1999; Duvel 1990; Fink and Reiner 2003). One of the main reasons is the increased lower-level shear between a southwesterly monsoon flow and northerly flow at the AEJ level (600 hPa).

Recently, Besson and Lemaître (2014) suggested that not only the midtropospheric AEJ and associated AEWs but also the upper-tropospheric TEJ might affect MCSs, mainly via its impact on upper-level divergence.

As shown in Fig. 2b, the TEJ can exhibit a distinct regional maximum over the coastal region of West Africa—even in the seasonal mean. On synoptic time scales, this maximum can be much more pronounced (Fig. 3a), giving it a similar appearance to jet streaks found at midlatitude jets.

According to quasigeostrophic theory, jet streaks are associated with substantial ageostrophic flows in their entrance and exit regions. In the idealized case of a straight jet streak in a flow with a Rossby number small in comparison to unity, theory predicts a symmetric four cell divergence–convergence pattern with upper-level divergence at the anticyclonic-shear side (poleward in case of an easterly jet) entry and cyclonic-shear side (equatorward) exit of a jet stream (e.g., Uccellini and Johnson 1979). The conditions for the development of a symmetric four cell pattern (shown in idealized form in Fig. 3b) are stringent and numerous factors including curvature of the jet axis and latent heat release strongly modulate the patterns of divergence and convergence. The four-cell pattern changes more toward a two-cell pattern if the Rossby number surpasses 0.5 (Van Tuyl and Young 1982). Given that the mean position of the TEJ ($\sim 6°$N) results in typical Rossby numbers around 0.7 [see calculation in Besson and Lemaître (2014)], a simple two-cell pattern might be the most realistic depiction. Substantial divergence can therefore only be expected at jet entrance regions. Besson and Lemaître (2014) linked divergence values of up to $3 \times 10^{-5}\,\mathrm{s}^{-1}$ to the entrance region of a pronounced TEJ streak. By integrating the continuity equation from the top (100 hPa) downward to 200 hPa, they then estimated maximal TEJ-related upward motion at about $10\,\mathrm{cm\,s}^{-1}$ in 200 hPa. For this computation, the aforementioned divergence value of $3 \times 10^{-5}\,\mathrm{s}^{-1}$ was assumed to be constant and the vertical velocity was set to zero at the tropopause.

It is, however, questionable whether possible jet streak–related upper-level divergence can be of any significance for convection over the Sahel. Most studies investigating the impact of jet streaks on convection focus on highly baroclinic jet configurations in midlatitude regions; there, the ageostrophic flow in the entrance region is often accompanied by a thermally direct, transverse circulation which is characterized by deep synoptic-scale ascent along sloped isentropes (e.g., Uccellini and Johnson 1979). Literature on jet streaks in tropical regions is sparse, however, likely because synoptic-scale dry ascent is assumed to be weak there due to the smallness of the Coriolis parameter (Charney 1963; Raymond et al. 2015). Therefore, it is unclear whether jet streaks at the TEJ also enable synoptic-scale ascent throughout the whole troposphere or whether the divergence-related mass deficit is compensated by
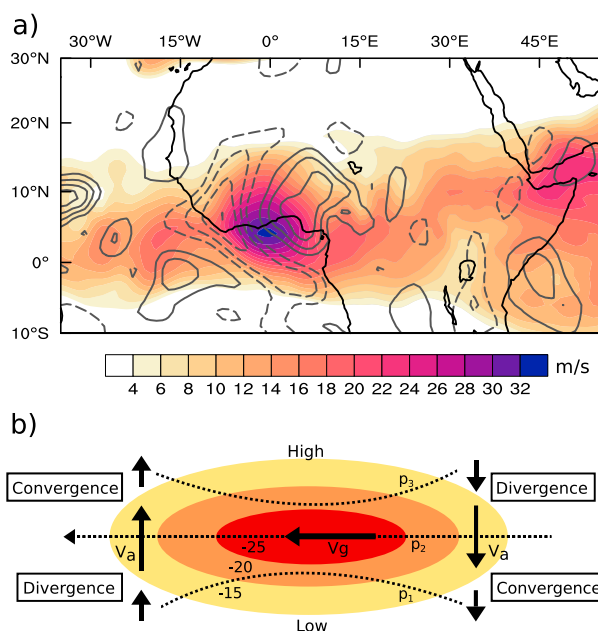

FIG. 3. Divergence pattern possibly associated with regional TEJ maxima: (a) 12-h averaged 200 hPa zonal wind field from ERA-Interim on 28 Aug 2009. Contours show anomalous divergence (solid) and convergence (dashed) with an interval of $5 \times 10^{-6}\,\mathrm{s}^{-1}$. (b) Sketch of the idealized situation at a straight easterly jet streak with the typical upper-level divergence at the right entry/left exit. Dashed lines depict isobares and the contours show isotaches.

convergence in layers directly below. In their in-depth case study, Besson and Lemaître (2014) described TEJ-forced ascending motions and associated adiabatic cooling reaching down as far as 4 km above ground level. Even if some TEJ-related uplift at the order of $\mathrm{cm\,s}^{-1}$ extends down to the boundary layer, it is certainly too weak to lift a potentially buoyant parcel to its LFC (Doswell 1987). Nonetheless, even weak synoptic-scale rising motion can be pivotal for convection in some cases. If it persists for at least some hours, synoptic-scale ascent preconditions the atmosphere through adiabatic cooling which increases CAPE and lowers CIN. Couvreux et al. (2012) have shown with idealized LES simulations that prescribed anomalies in large-scale midtropospheric ascent of only $2\,\mathrm{cm\,s}^{-1}$ can be a deciding factor for the initiation of convection in the semiarid Sahel region. Such cases might be rare, though, and the initiation of deep convection should mainly be controlled by thermodynamic factors and mesoscale dynamic forcing. In line with this thought, Besson and Lemaître (2014) ascribe TEJ streaks a subordinate role in convective initiation. They argue, however, that jet streak–related divergence may strongly benefit the organization and in particular the persistence of MCSs. Hence, a possible influence of the TEJ and embedded jet streaks on MCSs is still in debate which motivates our

more statistical analysis which will follow in the second part of this paper.

3. Data and methods

a. Statistical analysis of synoptic to intraseasonal variability

All statistical analyses described below are applied to a 32-yr-long (1979–2012; 1982 and 1985 are left out because of too many missing values) daily record of outgoing longwave radiation (OLR) measurements from NOAA (Lee 2014) and daily-averaged reanalysis output from ERA-Interim (Dee et al. 2011), NCEP–NCAR (Kalnay et al. 1996), MERRA-2 (Gelaro et al. 2017), and JRA-55 (Kobayashi et al. 2015) for the same time period. OLR is chosen as a suitable proxy for rainfall which is generally deemed to be valid in tropical regions where rainfall associated with deep convection predominates. All analyses are limited to the WAM season comprising JJAS.

First, power spectra for local and regional scales are calculated to identify typical time scales associated with most variation in OLR and wind speeds at the TEJ level (200 hPa). For this and the following analysis, regional averages for OLR are calculated from 15°W to 15°E over 8°–16°N, which represents the typical latitudinal extent of the WAM rain belt. For the TEJ, an averaging domain of the same size is used but shifted 6° to the south to account for the typical mean position of the TEJ core (6°N). To remove the signal of the annual cycle, daily-averaged data of each year are prepared by subtracting the first three harmonics of the respective annual cycle and an additional detrending. JJAS power spectra are then calculated for each year separately and averaged afterward. The spectral analysis is carried out using the NCL function specx_anal. Ten percent of the time series is tapered and some smoothing is applied by averaging three periodogram estimates. To check statistical significance of spectral peaks of the averaged spectra we calculate the best-fitting Markov spectrum and its lower 5% and upper 95% confidence bounds via the NCL function specx_ci. The Markov spectrum refers to a univariate lag-1 autoregressive process and can therefore represent white or red noise spectra. Spectral peaks that lie outside of the confidence bounds are considered to be significant because they differ from white or red noise.

Bandpass filtering is applied to the deseasonalized daily-averaged data to investigate the relationship between the TEJ and Sahel rainfall separately for three typical rainfall variability time scales: synoptic variability (2–8 days), submonthly variability (10–25 days) and MJO time scale variability (30–90 days). The bandpass filter used for all analyses in this study is a standard top hat spectral filter as implemented in the Climate Data Operators package (Schulzweida 2019). For each time scale, the JJAS lead–lag correlations between regionally averaged OLR and 200 hPa zonal wind are calculated individually for each year and averaged afterward. Before calculating the 10–25-day and the 30–90-day correlations, time series are smoothed by a 3-day running mean.

Spatial patterns of anomalous upper-level flow linked to Sahel convection anomalies on synoptic and submonthly time scales are explored via linear regression, similar to Kiladis and Weickmann (1997). Bandpass-filtered, spatially averaged OLR in a selected Sahel base region is regressed separately against the filtered zonal and meridional components of the 200 hPa wind and OLR itself for each grid point at different time lags. The linear dependence of circulation and OLR anomalies is then mapped by evaluating the respective regression equations for each grid point using one negative standard deviation in OLR at the base region as the independent variable. Statistical significances of the linear relationships are tested via a Student's t test that takes into account the reduction in the degrees of freedom due to autocorrelation.

b. Relationship between TEJ and MCSs

The possible relationship between the TEJ and initiation and further development of MCSs is explored by analyzing a large number of MCS initiations and associated upper-tropospheric dynamics. The focus is laid on large and organized MCSs because they are responsible for the bulk of rainfall and are more likely to interact with large-scale atmospheric dynamics than smaller, unorganized convection.

An objective MCS tracking algorithm developed by Huang (2017), based on the conventional area overlapping method combined with a Kalman filter, is applied to the Gridsat-B1 brightness temperature dataset (Knapp and Wilkins 2018). We use the traditional 233 K threshold to identify deep convective cells and demand that the 233 K isotherm encloses a minimum of $30\,000\,km^2$ (cloud shield radius $\gtrsim 100\,km$) and that the system has a lifetime of at least nine hours. This choice of minimum size and lifetime is justified for our purposes because MCS with radii $\geq 100\,km$ explain more than 80% of the MCS-associated integrated cloud cover according to Mathon and Laurent (2001). The same is true for systems with lifetimes $\geq 9\,h$. To prevent that a possible effect of the TEJ is overshadowed by precedent or adjacent MCS, each tracked MCS should represent a more or less isolated system that is neither the product of an MCS split nor directly triggered by systems nearby. For that, only those MCSs are selected for which no grid point with brightness temperature below 233 K is found three hours
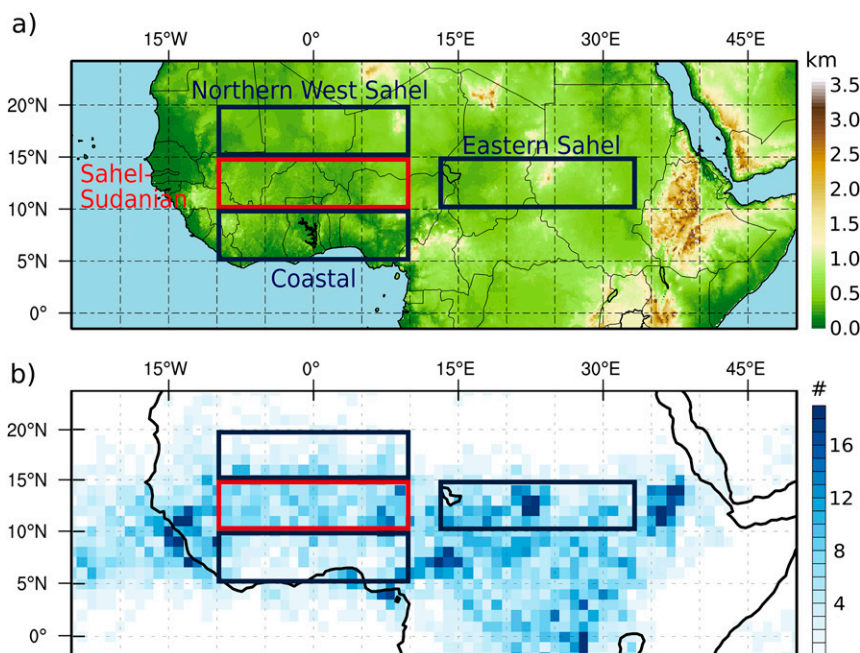
FIG. 4. (a) Topographic map of our study areas. The boxes show the chosen spatial composite regions. We lay the focus of our investigations on the mixed Sahel–Sudanian region, which is defined as a latitudinal band from 10° to 15°N spanning from 10°W to 10°E. (b) Initiations of large (maximum size $\geq$ 30 000 km^2) and long-lived (lifetime $\geq$ 9 h) Sahelian-type MCS per 1° $\times$ 1° grid boxes summed over 9 JJAS seasons (2007–15).

before initiation in a box of 5° longitudinal and 2° latitudinal extent east of the genesis area. In addition, each found event is required to be temporally separated by at least 24 h. As a consequence of these further selection criteria we exclude about 60% of all large Sahelian-type MCS initiations from our analysis which is a large but necessary trade-off to eliminate most effects from possible earlier or adjacent MCSs. Gradually relaxing these selection criteria and therefore increasing the number of examined MCS initiations leaves our results more blurred but mostly unchanged in their key aspects which is why we are confident that the selection of MCSs does not compromise the general validity of our study. The MCS tracking algorithm is applied for nine monsoon seasons (JJAS) between 2007 and 2015 (limited to the availability period of the Eumetsat divergence dataset which is described later) and found MCS genesis cases are binned into 1° $\times$ 1° grid boxes (Fig. 4b).

Assuming that surface characteristics and atmospheric dynamics do not differ fundamentally within a Sahel–Sudanian band between 10°W and 10°E and 10° and 15°N, we create a temporal and spatial composite of all MCSs initiated within this band in 9 years, such that all developing MCSs are now centered at the origin of a MCS genesis relative coordinate system. Because of the comparably high number of Sahelian-type MCSs and their large contribution to total rainfall there, we focus

on the Sahel–Sudanian region in our study but also examine MCS-related upper-tropospheric conditions in three other areas as depicted in Fig. 4a.

The resulting large MCS ensemble (287 MCS initiations in the Sahel–Sudanian region) enables a statistically robust investigation of mean synoptic conditions before, during and after initiation of MCSs and allows further to assess the range of conditions under which MCSs form. For the analysis of the atmospheric state, the output of the three reanalyses ERA-Interim, JRA-55, and MERRA-2 is used and compared among each other. In the case of ERA-Interim and JRA-55, 6-hourly output is interpolated to 3 h to match the temporal resolution of the MCS tracking. In the results section, most in-depth analysis is shown for ERA-Interim as it seems to resolve MCSs and their imprint on the synoptic-scale dynamics better than other reanalyses. OLR fields are displayed using the CERES SYN1deg OLR dataset (Rutan et al. 2015). Upper-level divergence is a crucial quantity for which we do not want to rely solely on reanalyses, as was the case in previous studies. Therefore we use the Eumetsat divergence product (EUMETSAT 2005) which is derived from satellite-derived atmospheric motion vectors (AMVs) and represents average divergence between 400 and 100 hPa. The calculation of AMVs in this product is based on the tracking of upper-level moisture features using successive satellite images of the water vapor
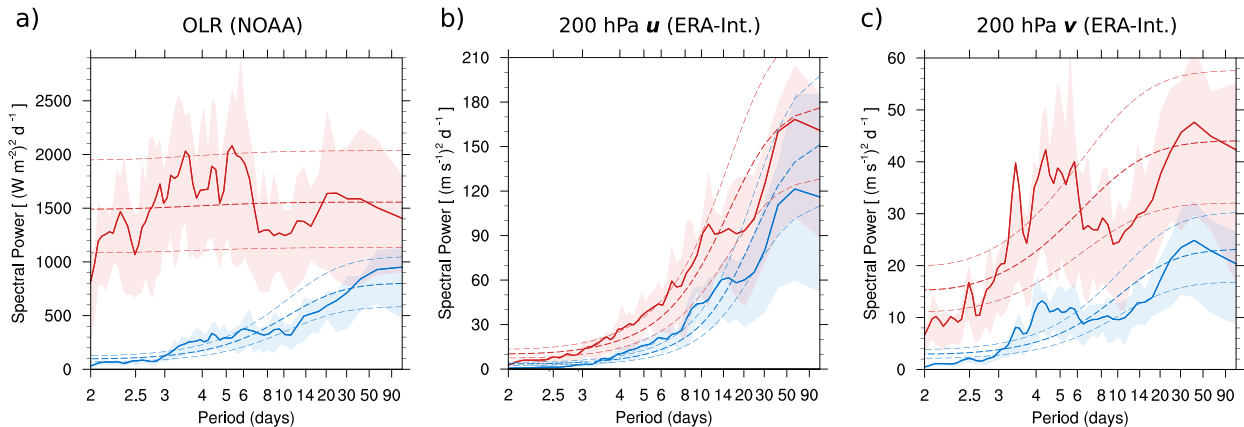
FIG. 5. Subseasonal power spectra for OLR, zonal, and meridional 200 hPa wind in the Sahel region. Thick lines show the averaged power spectra of 32 individual monsoon seasons for OLR, 200 hPa zonal wind, and 200 hPa meridional wind. Analysis is based on JJAS daily means of NOAA OLR from 1979 to 2012 and JJAS daily means of ERA-Interim 200 hPa wind from 1979 to 2012. Blue lines depict the regional variability as evaluated by a field mean (15°W–15°E, 8°–16°N for OLR, 15°W–15°E, 2°–10°N for zonal and meridional wind), red lines depict the local variability (at 12°N, 0°E for OLR, 6°N, 0°E for zonal and meridional wind). The light shading represents the respective interquartile range. As an indicator for significance, dashed lines show a theoretical Markov red noise spectrum with its 5th and 95th percentiles. The x axis is logarithmic.

channel (6.2 μm) of *Meteosat-8* at a 15 min interval. As a result, the derivation of AMVs and the subsequent calculation of upper-level divergence is not reliant on the presence of any clouds. The Eumetsat divergence product is available at spatial resolution of 1° and temporal resolution of 3 h for the years 2007–15. Although we consider the dataset to be sufficiently representative of the divergence at the TEJ level (200 hPa), we will designate it as $\overline{100\text{–}400\,\text{hPa}}$ divergence throughout the paper.

Anomalies analyzed in this part of the study are calculated as deviations from 12-day low-pass filtered values calculated separately for each 3-hourly time step of the day. This method provides a time of day dependent reference state which removes the signals of the diurnal cycle for the respective anomalies. The filtering cutoff period—12 days—is sufficiently above the time scales associated with MCS passages and synoptic-scale phenomena such as AEW (2–7 days) but short enough to exclude any effects from the seasonal cycle or the MJO. Statistical significance is assessed via a bootstrapping method of sampling with replacement using 5000 iterations.

4. Results

a. Statistical analysis of synoptic to intraseasonal variability

1) SPECTRAL VARIABILITY

If the TEJ and Sahel rainfall are assumed to interact on synoptic to intraseasonal time scales, similar distributions of spectral power would be expected. However, their respective 32-yr-averaged power density spectra exhibit substantial differences across all time scales. OLR displays highest spectral power in a period range between 3 and 7 days which is certainly associated with AEWs (Fig. 5a). Strongly apparent is the much higher local- than regional-scale variability (red versus blue lines) on synoptic time scales, likely due to the rather small-scale nature of convection. Beyond the synoptic time scale, the OLR spectrum shows, on average, no significant peaks in the 10–25-day band. For some years, however, a significant peak can be observed (see light shadings) which is likely associated with the QBZD and Sahel mode. A broader peak exists at the 30–90-day time scale which is hypothesized to be attributable to the MJO.

Compared to convection (OLR), the TEJ appears to be much more spatially homogeneous and its variability is confined to larger spatial and longer time scales. The power spectrum of zonal wind speed at 200 hPa resembles a red noise spectrum with no distinctive spectral peaks on shorter time scales (Fig. 5b). By far the strongest, albeit insignificant, variability can be observed at periods around 50 days. Contrary to the OLR power spectrum, the local scale variability is very similar to regional scale variability – even on very short time scales. Although highest spectral power is found on the MJO time scale, a broader significant signal exists between 4 and 15 days with some marked peaks at 9 and 14 days. A similar significant concentration of spectral power for such periods was found for symmetric OLR spectra as shown in Wheeler and Kiladis (1999, their Fig. 3), hinting at the substantial impact of equatorial waves (in particular Kelvin waves) on the TEJ variability.

In contrast to the zonal component of the TEJ, the power spectrum of the meridional wind in 200 hPa looks much more similar to the OLR spectrum with a strong peak at about 3.5 days and a broader maximum between 4 and 6 days (Fig. 5c). The broad maximum is consistent with the findings of Nicholson et al. (2007) who have shown that planetary waves with periods of 5–6 days are observed in the upper-tropospheric flow over West Africa. Furthermore, the aforementioned equatorial waves might explain a considerable portion of the variability of the 200 hPa meridional wind field.

2) CORRELATIONS ON ALL SYNOPTIC TO INTRASEASONAL TIME SCALES

We calculate—individually for each year—the lead–lag correlation between daily Sahel region averages of OLR (averaged from 15°W to 15°E and 8° to 16°N) and 200 hPa zonal wind (averaged from 15°W to 15°E and 2° to 10°N). A positive correlation coefficient means that increased convection (negative OLR anomaly) goes along with an increased TEJ speed (negative zonal wind anomaly). When a maximal positive correlation is observed at positive time lags, it indicates that phases of an intensified TEJ lag phases of stronger convective activity.

For synoptic time scales, by far the highest 32-yr averaged correlation of 0.28 is observed when OLR anomalies lead TEJ anomalies by one or two days (Fig. 6a), meaning that an intensified TEJ is mostly observed after a period of increased convective activity and not vice versa. On time scales between 10 and 90 days, the lead–lag correlations remain below 0.3—without pronounced peak values—and therefore do not surpass the distinct maximum value found for synoptic time scales. The relationship on the MJO time scale is characterized by a broad interval of significant correlations of up to 0.28 from −4 to +4 days (Fig. 6c). On the submonthly time scale, the only barely significant positive correlation of 0.2 is observed at a time lag of +3 (Fig. 6b). Significant westerly anomalies at 200 hPa and therefore a weakening of the TEJ are observed 1 day before maximum convection on synoptic and some 5 days prior on submonthly time scales. While it is clear for synoptic time scales, the significance of the found lead–lag relationships is doubtful for the submonthly and MJO time scale. In particular on the MJO time scale, there are no distinct peaks in the correlogram which could indicate a clear lead–lag relationship. Moreover, the OLR–TEJ relationship on both time scales between 10 and 90 days exhibits a strong interannual and decadal variability such that in about 20%–25% of all years the correlation becomes negative at time lags from +1 to +3 (bar plots at bottom of Figs. 6b,c).

The main findings regarding maximum correlations and corresponding time lags are consistent among all reanalyses (Table 1). We further test the sensitivity of the lead–lag relationships against the area and position of the region over which the spatial averages are calculated. There are no major contradictions to the results presented: smaller averaging boxes, small latitudinal shifts or a change of the latitudinal shift between the boxes result in lower correlations, but the most important result, which is that the TEJ generally lags convection anomalies, is unchanged (not shown).

For a better understanding of the lead–lag relationships, the next two subsections present upper-tropospheric circulation patterns associated with Sahel convection anomalies on synoptic and submonthly time scales. The MJO time scale will not be discussed because the OLR regression pattern on the selected Sahel base region OLR is nearly identical to the MJO in phase 1 as depicted in Alaka and Maloney (2012, their Fig. 6). During this phase, increased convective activity over West Africa co-occurs with increased upper-level easterlies about the equator which can be understood as an equatorial Rossby wave response to anomalous heating over the equatorial Indian Ocean. Although the strength of the anomalous easterlies decreases exponentially from the equator, some significant anomalies extend northward to about 10°N. These remotely induced anomalies that co-occur with increased convection over the Sahel may explain the significant correlations on the MJO time scale at time steps −4 to +4.

3) DOMINANT SPATIAL PATTERNS ON THE SYNOPTIC TIME SCALE (2–8 DAYS)

The spatiotemporal analysis of the Sahel rainfall–TEJ relationship on the synoptic time scale (2–8 days) shows—in agreement to the previously found lead–lag relationship—that periods with a stronger TEJ (i.e., negative 200 hPa zonal wind anomalies) seem to lag periods of increased convection. These results are obtained by regressing OLR and 200 hPa circulation anomalies on the 2–8 days bandpass-filtered OLR values in the selected Sahel base region (red box in Fig. 7). Without any imposed time lag (at day 0), the OLR regression pattern shows a negative OLR anomaly of up to 30 W m^{-2} (Fig. 7a). The negative OLR signal appears to be embedded in an AEW-like structure as it is associated with a significant lower- and midtropospheric wind anomaly pattern akin to AEW composites as presented in Kiladis et al. (2006, their Fig. 3) (not shown). Upper-tropospheric wind anomalies (here we show ERA-Interim) at day 0 can be identified as mostly divergent outflow with westerly anomalies behind and easterly anomalies ahead of the OLR signal (Fig. 7b).
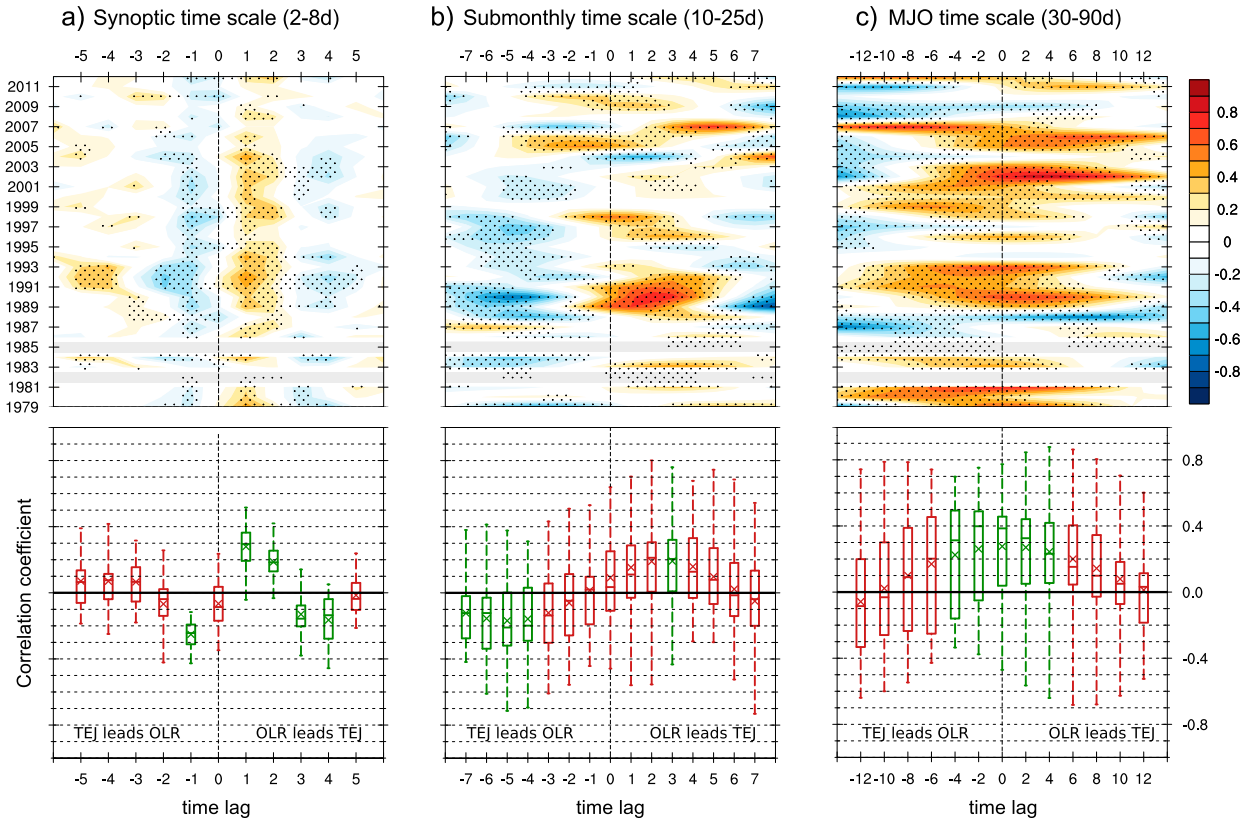
FIG. 6. Relationship between regional TEJ intensity and convective activity in the Sahel over a range of synoptic to intraseasonal time scales. (top) Lead–lag correlations between OLR and 200 hPa zonal wind throughout 32 years. A positive correlation coefficient means that increased convection (negative OLR anomaly) goes along with increased TEJ speed (negative zonal wind anomaly) or vice versa. Positive correlations observed at positive time lags indicate that phases of an intensified TEJ lag phases of stronger convective activity. The correlations are calculated separately for each year from daily bandpass-filtered JJAS data of regionally averaged OLR (15°W–15°E and 8°–16°N) and 200 hPa zonal wind (averaged from 15°W to 15°E and 2° to 10°N). Stippling indicates statistical significance at the 5% level determined by a bootstrapping test with 5000 iterations. (bottom) Box-and-whisker plots for the corresponding minima and maxima; the 25%, 50%, and 75% quartiles; and the average (crosses) of the correlation coefficients. Positive lag means that changes in OLR lead changes in 200 hPa zonal wind. The green color of the boxes denotes time lags for that the average correlation is statistically significant at the 5% level (determined by a bootstrapping test with 5000 iterations).

One day later the OLR signal moves westward by about 5°, accompanied by a significant decrease of its amplitude to less than $-10 \, W \, m^{-2}$. During this time, a significant 200 hPa easterly anomaly of about $0.5 \, m \, s^{-1}$ evolves near the selected Sahel base region where the OLR signal reached its maximum amplitude two days earlier. In addition, a zonally elongated easterly anomaly of up to $0.8 \, m \, s^{-1}$ appears near the equator. After two days, the OLR anomaly dissipates but the easterly anomalies at the TEJ level still persist.

Before the appearance of the negative OLR anomaly, the TEJ does not show any striking features besides a weakening near the Guinean coast. A jet streak–like pattern is neither observed in the mean state nor in the anomalies. The anomalous 200 hPa geopotential field is characterized by a westward-propagating wavelike pattern (Fig. 7c). At a time lag of −1 day, widespread

cross-equatorial southerlies are observed in relation to that wave structure. Given an approximate frequency of 5 days, a wavelength of about 6000 km and the typical cross-equatorial flow associated with geopotential anomalies roughly asymmetrical about the equator, the observed wave pattern appears to be related to a mixed

TABLE 1. Maximal 32-yr averaged lead–lag correlations and corresponding time lags (in days) between OLR (NOAA) and 200 hPa zonal wind on synoptic to intraseasonal time scales for all reanalyses. Positive time lag means that changes in OLR lead changes in 200 hPa zonal wind.

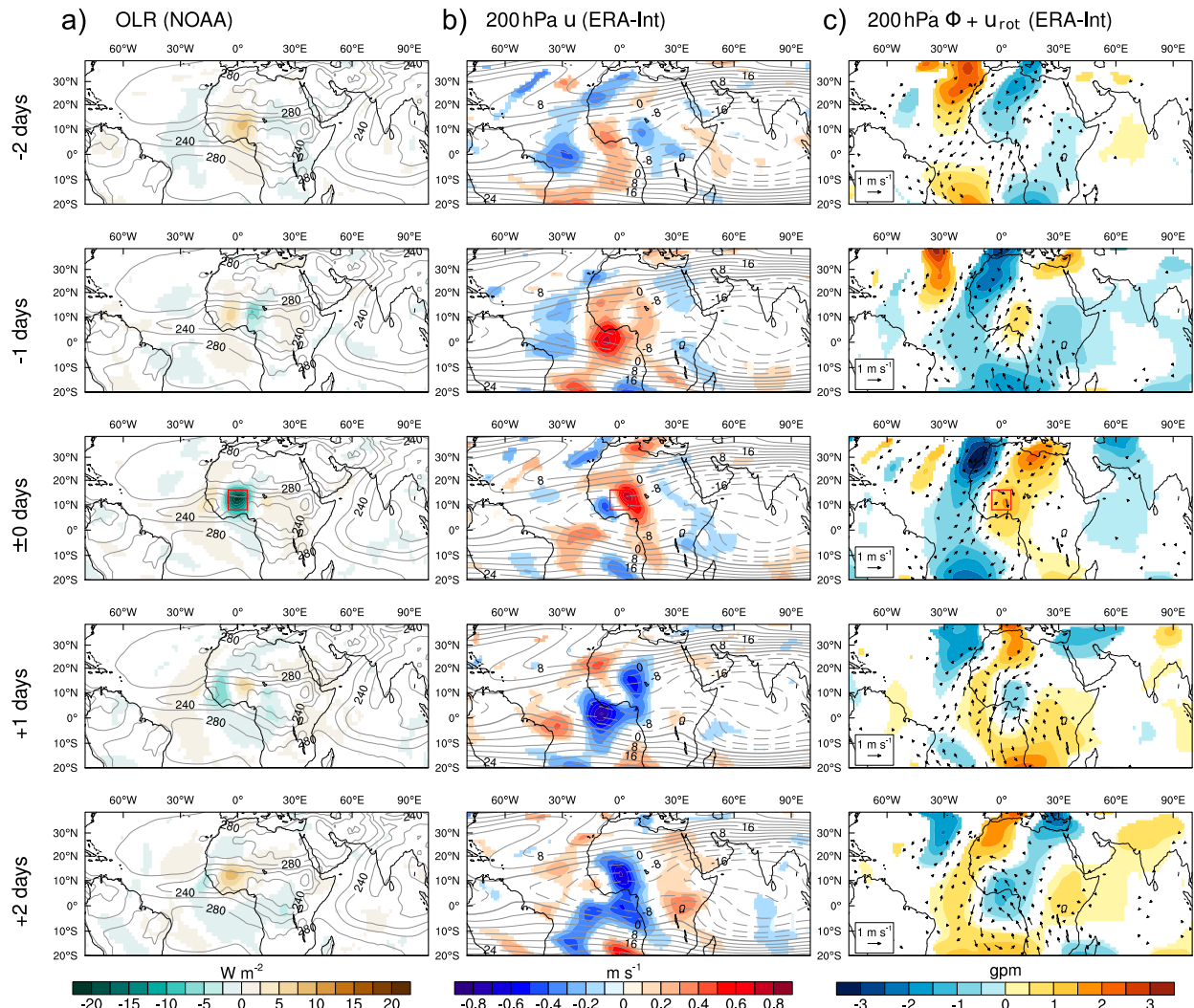|	2–8 days	10–25 days	30–90 days
ERA-Interim	0.28 + 1	0.19 + 3	0.28 + 0
NCEP–NCAR	0.24 + 1	0.15 + 3	0.23 −1
MERRA-2	0.28 + 1	0.22 + 2	0.26 + 0
JRA-55	0.27 + 1	0.18 + 2	0.27 + 1

FIG. 7. OLR and 200 hPa circulation features associated with synoptic-scale anomalies of Sahel convection. (a) 2–8-day bandpass-filtered OLR anomalies predicted by linear regression using one negative standard deviation in 2–8-day bandpass-filtered OLR at the base region (red box) as independent variable. (b) Corresponding 2–8-day filtered anomalies of 200 hPa zonal wind u. (c) Corresponding 2–8-day filtered anomalies of bandpass-filtered 200 hPa geopotential (Φ) and nondivergent wind ($\mathbf{u}_{rot}$) anomalies. Each row has a designated time lag, going from -2 days to $+2$ days. All anomalies shown (including wind vectors) are statistically significant at the 5% level determined by bootstrapping method with 1000 iterations.

Rossby gravity wave (e.g., Matsuno 1966; Yang et al. 2007; Kiladis et al. 2009).

4) DOMINANT SPATIAL PATTERNS ON THE SUBMONTHLY TIME SCALE (10–25 DAYS)

On the submonthly time scale (10–25 days) the OLR field regressed on OLR in the Sahel base region shows a pattern that might be interpreted as the weighted superposition of the Sahel mode (Sultan et al. 2003) and the QBZD (Mounier et al. 2008). For the selected Sahel base region which represents the average extent of the main monsoon rainbelt, the Sahel mode is more strongly present than the QBDZ. At day 0, a large region

spanning from Africa's west coast to about 20°E and from the Gulf of Guinea up to the northern Sahel is covered by OLR anomalies of up to $-8\,\text{W}\,\text{m}^{-2}$ (Fig. 8a). Four days prior to the OLR minimum over the Sahel, the first significant negative OLR anomaly appears over the central and eastern Sahel. This convective signal travels westward while strengthening until reaching maximum amplitude over the Sahel region.

Upper-tropospheric circulation changes associated with one negative standard deviation of OLR are mostly constrained to the coastal region and the Northern Sahel region (Fig. 8b). The TEJ remains mostly unchanged. At a time lag of -2 days, an easterly anomaly first appears
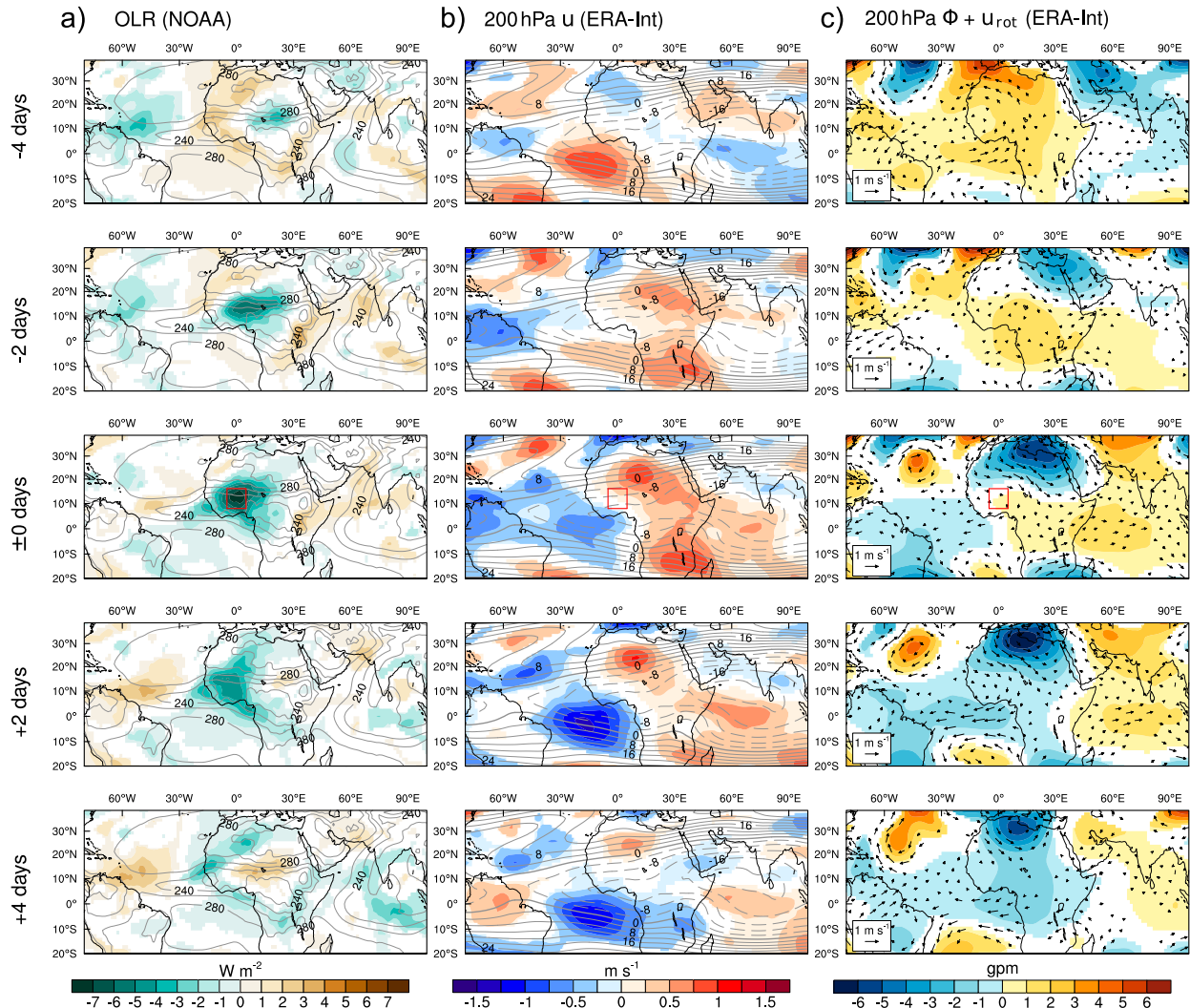
FIG. 8. OLR and 200 hPa circulation features associated with anomalies of Sahel convection on the submonthly time scale. (a) 10–25-day bandpass-filtered OLR anomalies predicted by linear regression using one negative standard deviation in 10–25-day bandpass-filtered OLR at the base region (red box) as independent variable. (b) Corresponding 10–25-day filtered anomalies of 200 hPa zonal wind u. (c) Corresponding 10–25-day filtered anomalies of bandpass-filtered 200 hPa geopotential (Φ) and nondivergent wind ($\mathbf{u}_{rot}$) anomalies. Each row has a designated time lag, going from -2 days to $+2$ days. All anomalies shown (including wind vectors) are statistically significant at the 5% level determined by bootstrapping method with 1000 iterations.

over northeastern Brazil. This signal moves eastward and reaches maximum amplitude of about $-1.5\,\mathrm{m\,s^{-1}}$ over the equatorial Atlantic at a time lag of $+2$ days. Although this signal does not reach further northward than 10°N, it might explain the low, albeit significant positive lag correlation between 200 hPa zonal wind and OLR in the Sahel region on this time scale. Two days later, the eastward movement seems to come to a halt and the amplitude weakens. The described equatorial and eastward-traveling 200 hPa easterly anomaly is likely associated with the QBDZ although this mode of biweekly convection is much less visible in the OLR field. When the OLR base region is shifted further to the south, the

regressed OLR pattern resembles more and more the QBDZ as described in Mounier et al. (2008). The corresponding upper-level circulation features are then mostly confined to the equator and are identifiable as the eastward-propagating Kelvin wave-like anomalies related to the Walker-type circulation across the Atlantic.

In synopsis, the statistical analysis of the spatiotemporal relationship between Sahel convection and TEJ intensity for synoptic and submonthly time scales yields a clear result: Consistent among all reanalysis models, there is no indication that phases of increased convective activity are preceded by an anomalously strong TEJ or a jet streak pattern. Upper-level easterlies are increased

south of increased convection after one or two days which is in accordance with the maximum lag correlation found in the previous section. These findings are in good agreement with one key result of Kiladis and Weickmann (1997) who explored the relationship between upper-tropospheric circulation and convective activity in tropical regions on the 6–30-day time scale: in regions with persistent upper-level easterlies, which includes the Sahel region, upper-tropospheric circulation anomalies are induced by anomalous convective activity, and not vice versa.

b. Relationship between TEJ and MCS

1) ATMOSPHERIC CONDITIONS BEFORE MCS GENESIS

Initiation of deep convection is complex and demands the simultaneous presence of many ingredients. The primary aim of this section, however, is not to unravel the complex interplay of all involved processes but to analyze upper-level winds before MCS initiation within a more complete statistical approach than Besson and Lemaître (2014). Following this investigation, a brief analysis of the most important mid- and lower-tropospheric processes will be presented.

Figure 9 shows the composite-averaged OLR (CERES SYN1deg) anomaly of 287 newly forming MCSs and associated anomalies of dynamical quantities (ERA-Interim) in form of latitude–longitude maps centered on a common, initiation-relative grid over the course of 24 h, beginning with the situation 6 h before initiation (top row) and ending with the dissipation stage (bottom row). Maximal negative OLR anomalies of about $70 \, \mathrm{W \, m^{-2}}$ are observed 3 or 6 h after initiation which is consistent with the widespread and vigorous deep convection in the early mature MCS stage (Fig. 9a). The TEJ, depicted by anomalous 200 hPa ERA-Interim zonal winds, shows on average no distinct features in the 6 h before MCS initiation (Fig. 9b). Only a westerly wind anomaly of up to $1 \, \mathrm{m \, s^{-1}}$, which later becomes significant, is found slightly southwest of the future MCS genesis region. A weak but significant southerly anomaly of $0.5 \, \mathrm{m \, s^{-1}}$ is observed at 200 hPa east of the formation region shortly before MCS initiation (Figs. 9b, 10k). Although the signals in the composite means are weak, the high variability of upper-level wind anomalies among all 287 composite members should be stressed. In a $2° \times 2°$ box around the MCS initiation area, the 200 hPa easterly wind anomaly before initiation ranges from roughly -10 to $+10 \, \mathrm{m \, s^{-1}}$ (Fig. 10h, blue line; please note the scaling factor applied to the 10th–90th percentile range).

Consistent with the composite-averaged anomalous wind field in the ERA-Interim reanalysis, the Eumetsat divergence product shows a small but significant upper-tropospheric convergence anomaly in the MCS initiation area (Fig. 9c). This anomalous convergence is observed over 24 h before MCS formation in both the Eumetsat and ERA-Interim datasets (Figs. 10b,c). Ensemble-wide evaluation of absolute Eumetsat divergence averaged over 6 h before MCS genesis and spatially averaged within a $2° \times 2°$ box centered at the MCS genesis location yields: only 26% of all 287 MCSs are initiated under large-scale upper-level divergence exceeding the climatological summer mean of that area. Substantial divergence values larger than $5 \times 10^{-6} \, \mathrm{s^{-1}}$ only appear in 18% of all cases, values above $10^{-5} \, \mathrm{s^{-1}}$ exist in only 6% of all cases. Divergence as high as $3 \times 10^{-5} \, \mathrm{s^{-1}}$ is not observed before MCS genesis. Besson and Lemaître (2014) reported such a value as solely induced by a TEJ streak. In our analysis based on satellite-derived divergence, such high values are only observed after MCS initiation as a result of the MCSs' convective outflow. The analysis in Besson and Lemaître (2014) relied exclusively on reanalyses and the higher divergence values could therefore have been a consequence of spurious convection.

Albeit less pronounced in the upper-level divergence (Fig. 10d), the aforementioned variability in the upper-level winds before MCS genesis motivates a deeper analysis of the entire MCS ensemble. A nonnegligible number of cases could exist in which an anomalous TEJ and/or a distinct jet streak might exert an effect on the organization of MCSs. This hypothesis is tested by plotting key parameters (size, lifetime, intensity, speed) of each of the 287 MCSs against the large-scale Eumetsat divergence anomaly averaged over the 6 h before MCS initiation in a box slightly upstream (1°W–3°E, 2°S–2°N) of the future MCS genesis location. Preexisting upper-level divergence seems to have no substantial effect on organization of MCSs. All scatterplots strongly resemble random distributions with no apparent clusters (Figs. 11a–d). The correlations between preceding anomalous upper-level divergence and all MCS parameters are low and statistically insignificant ($p > 0.05$). To gain further insight, the noise of the anomalous $\overline{100\text{–}400 \, \mathrm{hPa}}$ divergence field is filtered out by only considering substantial deviations from the median. For this, only those data points are selected that lie either below the first or above the second tertile with respect to both the anomalous divergence and the respective MCS parameter (shaded outer quadrants in Figs. 11a–d). It is then counted how often distinctly above or below median MCS parameters values co-occur with substantially increased or decreased preceding upper-level divergence. This procedure is repeated
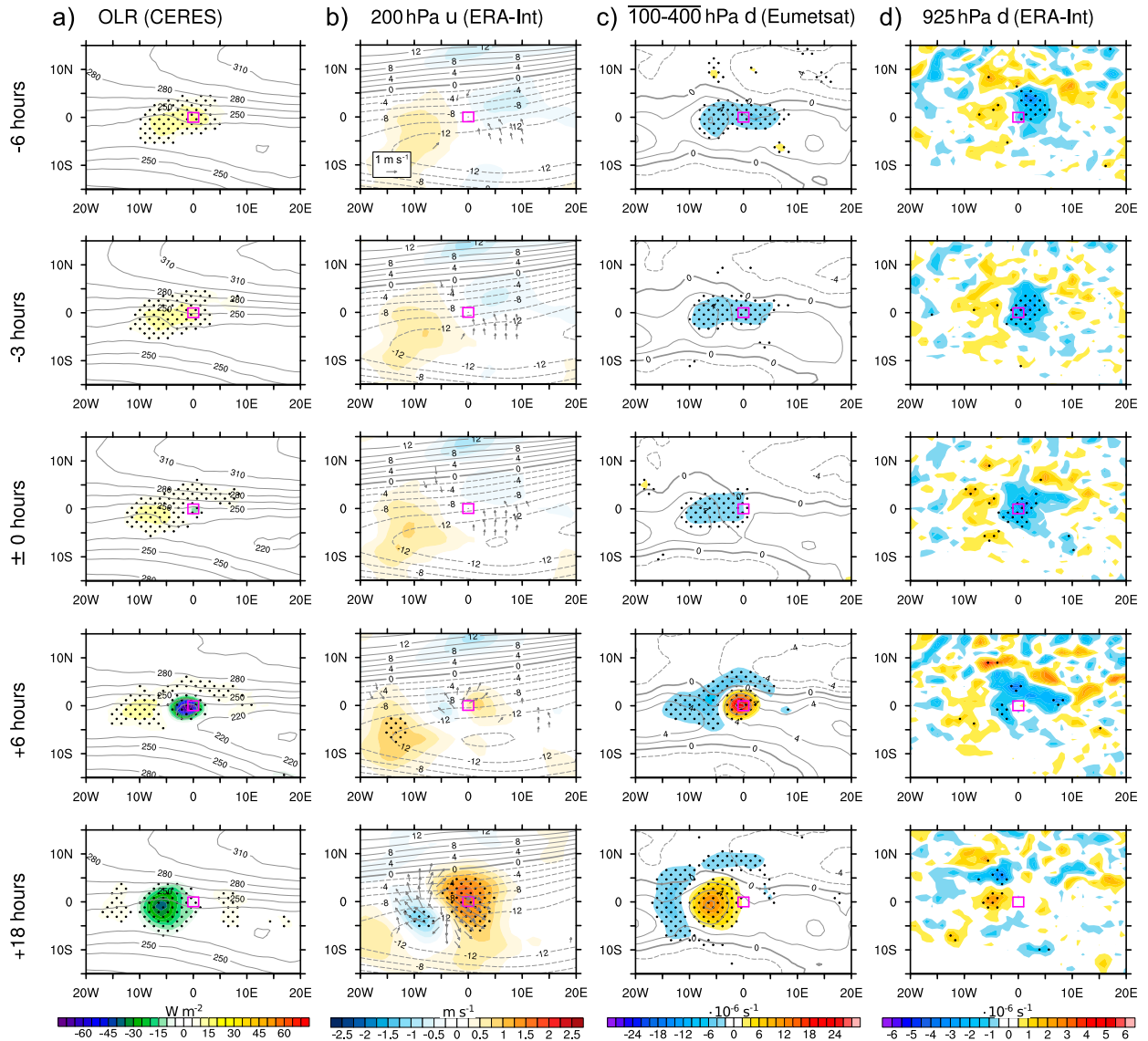
FIG. 9. MCS initiation centered relative latitude–longitude maps of composite mean anomalies (average over 287 MCS initiation cases in the Sahel–Sudanian region) of OLR (CERES), 200 hPa zonal wind u (shaded) and significant 200 hPa wind vectors (both ERA-Interim), upper-tropospheric $\overline{100\text{–}400}$ hPa divergence d (Eumetsat), and 925 hPa divergence d (ERA-Interim). Anomalies are calculated against the time of day reference state obtained by 12-day low-pass filtering (shown with contour lines except for 925 hPa convergence). Rows designate different time lag/lead relative to the time of MCS genesis. The small magenta box is a visual aid depicting the MCS genesis area. Dots indicate statistical significance at the 5% level tested by bootstrapping with 5000 iterations.

for 5000 times after resampling the data each time. According to this method, above-median MCS lifetime, size, intensity, or movement speed are not significantly more frequent in situations with preexisting anomalous divergence at the TEJ level.

The same scatterplot analysis is carried out for a jet streak measure to guarantee that possible jet-induced divergence is not overshadowed by other effects. Inspired by the conceptual jet streak picture depicted in Besson and Lemaître (2014, their Fig. 7a), we define the

jet streak measure as the spatially averaged 200 hPa zonal wind anomaly in a region slightly ahead and south (10°W–0°E, 4°S–2°N) of the MCS genesis location from which the average zonal wind anomaly in a larger area (15°W–15°E, 5°S–5°N) is subtracted. In a further test, the relationship between the local TEJ intensity and MCS parameters is investigated for a possible effect of upper-level wind shear on MCS organization. As was the case before with upper-level divergence, no significant statistical connection is found between any MCS parameter
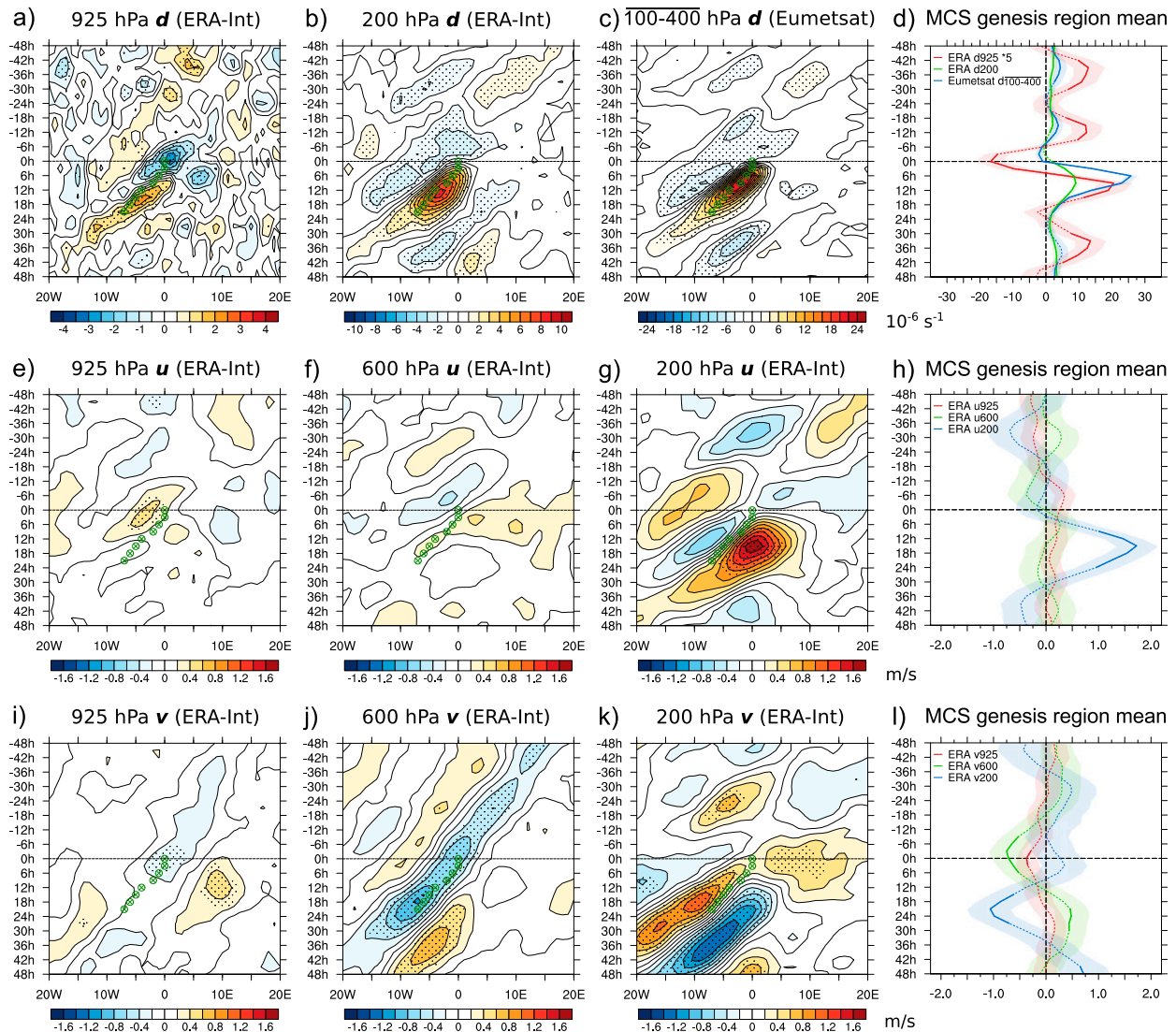
FIG. 10. Hovmöller plots of several composite mean anomalies (average over 287 MCS initiation cases in the Sahel–Sudanian region). Dots indicate statistical significance at the 5% level tested by bootstrapping with 5000 iterations. Crosses depict the path of the composite MCS. The right column shows the course in time for the initiation location field mean ($2° \times 2°$ box) of the three quantities within each row. The 925 hPa divergence from ERA-Interim has been scaled up by a factor of 5 for better visibility. The shaded areas around the lines depict the 10th and 90th percentiles scaled by a factor of 0.1. Solid line parts denote statistical significance at the 5% level.

and these two TEJ-related measures (not shown). This result further indicates that the TEJ plays no major role for MCS organization, at least not by affecting upper-level shear or divergence.

Beyond the scope of upper-tropospheric dynamics, there is mostly agreement with earlier studies: The composite-averaged MCS forms within a significant preexisting wavelike pattern at 600 hPa which moves westward at a speed of approximately $6.5\,\mathrm{m\,s^{-1}}$ and might be associated with an AEW (Fig. 10j). Average initiation within the northerly wind anomaly ahead of the AEW trough would be in agreement with previous

studies that found that West Sahelian MCSs are most frequent in this wave sector (Diedhiou et al. 1999; Duvel 1990; Fink and Reiner 2003). Because MCSs can also be initiated in each other sector of an AEW or without the presence of AEWs, the composite mean does not show a coherent AEW-like circulation structure (not shown). Prior to initiation, AEJ speed is on average increased by nearly $1\,\mathrm{m\,s^{-1}}$ ahead and slightly south of the future genesis area (Fig. 10f; anomaly is less pronounced in the Hovmöller plot). This observation, although just missing the 5% significance level, stands in contrast with the favorable dynamical configuration between the AEJ
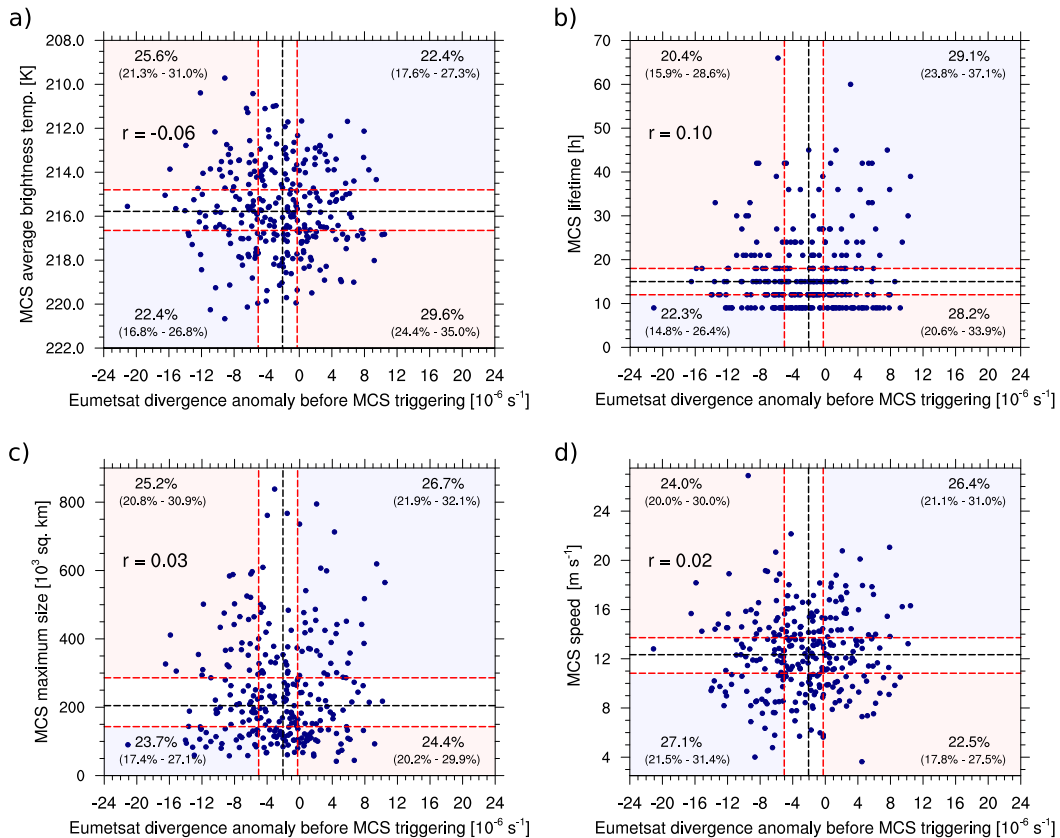
FIG. 11. Relationship between preexisting large-scale divergence and several MCS parameters characterizing its degree of organization for the ensemble of 287 MCSs in the Sahel–Sudanian region. Scatterplots showing the (a) MCS intensity (average brightness temperature), (b) MCS lifetime, (c) MCS maximal size, and (d) MCS travel speed as a function of anomalous large-scale divergence 6 h prior to MCS genesis. The horizontal black line shows the median value of the respective MCS quantity, the black vertical line represents the median for the preceding divergence anomaly. Red lines depict the respective tertiles for the MCS quantity and preceding divergence. The percentage values express the relative frequency of MCS for each of the four outer quadrants which are bounded by the horizontal and vertical red lines (and marked by the light shading). The percentages in parentheses denote the 5% and 95% confidence bound determined by a bootstrapping routine with 5000 iterations. If 25% is not within this span, we assume that above/below median MCS parameter values are significantly more/less often observed in the respective quadrant.

and well-organized MCSs as proposed in Besson and Lemaître (2014). Even though many typical mesoscale convergence lines are not resolved, all reanalyses show a significant increase of large-scale low-level convergence some hours before MCS initiation (Figs. 9d, 10a). This increase in low-level convergence might be a spurious artifact of the reanalysis assimilation scheme but could also be associated with a shallow convection phase preceding deep convection. Consistent with the convergent low-level flow, ERA-Interim shows an anomalously cyclonic near-surface circulation with slightly albeit significantly increased monsoon flow to the west, increased northerly flow at and stronger southerly flow behind the MCS genesis region (Figs. 10e,i). Associated with that cyclonic circulation is a noticeable, albeit nonsignificant decrease in 925 hPa geopotential height.

Significantly higher CAPE values and a significant mainly temperature related increase of moist static energy in lower levels are present before the MCS forms (not shown). Orography is another crucial forcing, since according to Mathon and Laurent (2001), 55% of MCSs develop in regions above 400 m. Although the selected Sahel–Sudanian region is rather flat and not crossed by prominent mountain ranges, slightly more MCS initiations are detected at or near elevated terrain. Roughly 30% of MCS are initiated in regions above 400 m (topography data at 0.25° resolution) but these regions take up only 22% of the study area (not shown).

In summary, the investigation of nearly 300 Sahelian MCSs shows that the initiation is generally not associated with jet streak–like configurations or any striking anomalies in the upper-tropospheric wind field.

Substantial upper-tropospheric divergence exceeding climatological mean values is only present in 26% of all examined MCS initiations. There is further no significant relationship between preexisting TEJ-related divergence and intensity, size or longevity of MCSs. A brief analysis beyond the scope of upper-tropospheric dynamics confirms the important role of orography, favorable local-scale thermodynamic conditions and low- to midlevel dynamical forcing. What cannot be excluded within the scope of this analysis are possible interactions between the TEJ and some of the abovementioned forcings.

2) MODIFICATION OF THE TEJ BY MCSS

Some hours after initiation, the MCS develops a typical upper-level outflow anticyclone. North of the MCS, where the Coriolis force is higher, we observe a stronger westerly anomaly in the northeastern sector of the MCS compared to a weaker easterly anomaly in the southwestern sector. Weak southerly anomalies are found in the northwestern sector and stronger northerly anomalies exist in the southeastern sector (Figs. 9b, 10g,k). Albeit significant, the modification of the TEJ is rather weak in the composite mean because averaging of a high number of different MCS cases acts as rather heavy spatial smoothing. For some single cases, though, a strong easterly anomaly of up to $5\,\mathrm{m\,s}^{-1}$ is found in the southwest sector of the MCS (not shown), which is in good agreement with the results of numerical simulations in Diongue et al. (2002). They found that an MCS' vigorous equatorward outflow deflected to the right by the Coriolis force can result in a significant intensification of the TEJ of about $15\,\mathrm{m\,s}^{-1}$ over scales of hundreds of kilometers. This regional intensification might lead to a marked jet streak–like appearance in the regional 200 hPa zonal wind field.

3) COMPARISON BETWEEN DIFFERENT MCS INITIATION REGIONS AND REANALYSES

Composite-averaged upper-tropospheric winds before MCS initiation are similar for all other examined African regions. As in the main study area, the Sahel–Sudanian zone, no significant anomalies in upper-level zonal wind speed are found near the MCS genesis area on average (Figs. 12a,d). Significant upper-level convergence and descending motion is apparent in all regions some 12–24 h before MCS initiation (Figs. 12c,d). Moreover, no statistical evidence is found that preceding jet anomalies and associated upper-level divergence affects MCS intensity, lifetime or maximum size in any of the selected regions (not shown). With the exception of the northern Sahel, no significant meridional wind anomalies are present in the upper troposphere before MCS initiation. The main

difference between the four regions is the involvement of AEWs. In the eastern Sahel region many AEWs are weaker, have not formed yet or might be initiated later by strong MCSs (Fig. 12b).

The consistency of our findings is further tested by comparing MCS-associated mean atmospheric fields of ERA-Interim to those of MERRA-2 and JRA-55 for the Sahel–Sudanian region (not shown). High agreement among all three reanalyses is found for the atmospheric conditions before MCS genesis. None of the reanalyses show significant zonal wind anomalies or any significant divergence at the TEJ level. In synopsis, the comparison between different regions and different reanalyses provides further strong evidence that MCS initiation and organization are not associated with significant TEJ anomalies.

5. Summary and concluding discussion

Previous studies found a significant positive correlation between the strength of the TEJ over West Africa and Sahel rainfall on decadal and interannual time scales. A causal relationship was suggested but it has been unclear whether substantial interaction exists on much shorter time scales. In the first part of this study, we therefore investigate the relationship between the West African TEJ and Sahel rainfall (using OLR as proxy) over a range of synoptic to intraseasonal time scales. Using a variety of statistical analyses, we find the following:

- The statistical relationship between the intensity of the West African TEJ and convective activity in the Sahel is much weaker on synoptic to intraseasonal (correlations below 0.3) than on interannual and decadal time scales (correlations between 0.5 and 0.9)
- On synoptic time scales, phases of anomalous convective activity significantly lead changes in the regional TEJ intensity by one or two days, suggesting that convection anomalies are more likely to cause changes in the regional TEJ than vice versa

A weaker statistical connection on shorter time scales is expected because high-frequency noise is not filtered out, as is the case for correlations calculated on longer multiyear time scales. Therefore, a strong relationship between the TEJ and Sahel rainfall might only be reflected in seasonal averages; one could assume a mainly one-way interaction in which the seasonally integrated effect of excess rainfall results in a stronger than normal TEJ over West Africa. However, the question arises as to whether the strong statistical correlation on longer time scales is mainly explained by such a direct relationship or whether a ''third variable'' considerably
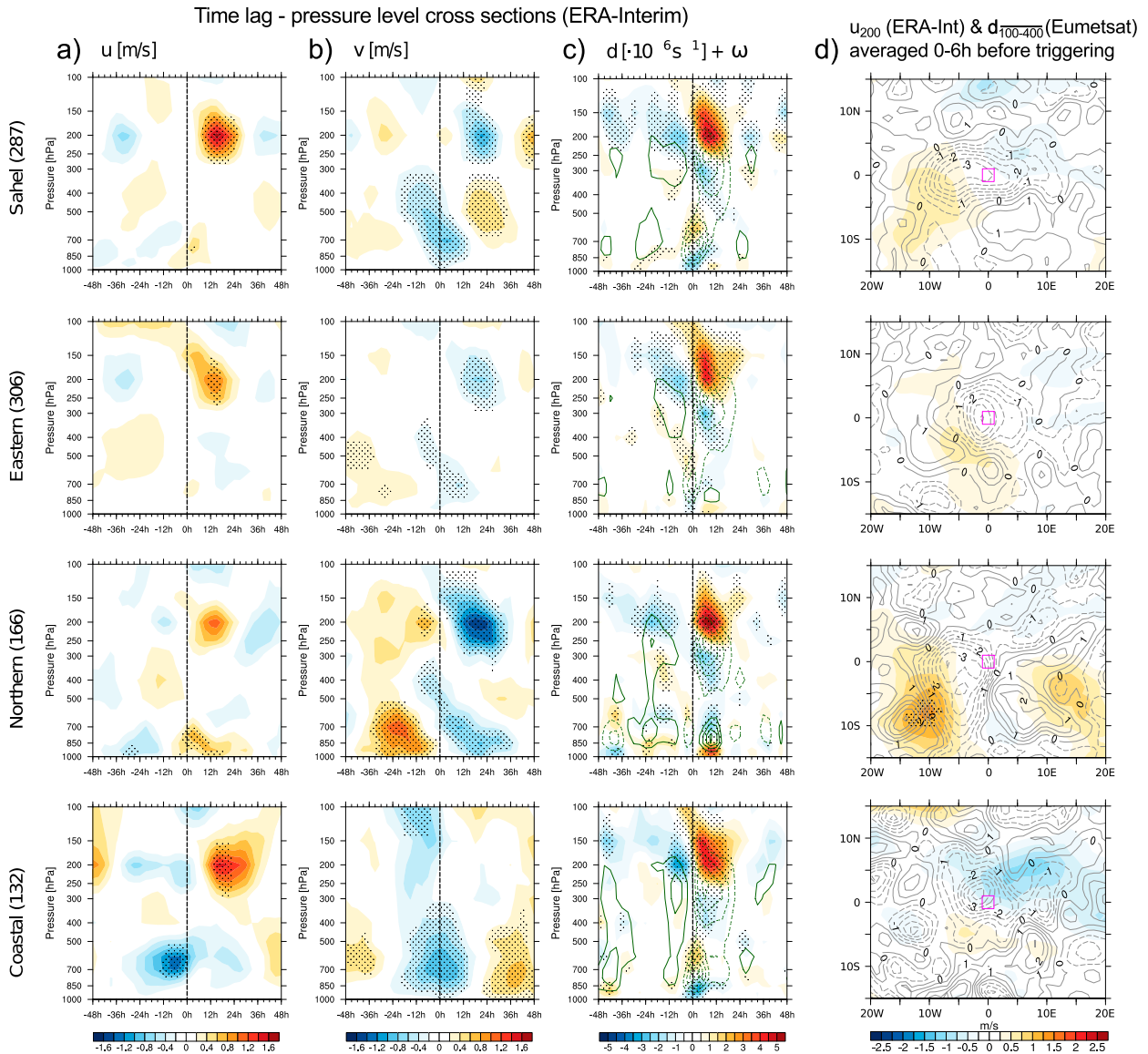
FIG. 12. Comparison of atmospheric conditions before MCS genesis between different regions. First three columns from the left show time lag–pressure level plots of composite mean anomalies for the $2° \times 2°$ area mean around the MCS initiation location for the quantities (from left to right): zonal wind u, meridional wind v, divergence d (shaded) + vertical motion ω (contour interval: 0.01 Pa s^{-1}, dashed contours depict ascent) from the ERA-Interim dataset. The rightmost column depicts longitude–latitude plots of ERA-Interim 200 hPa zonal wind anomalies (shaded) and Eumetsat $\overline{100\text{–}400\,\text{hPa}}$ divergence anomalies (contours every $0.5 \times 10^{-6}\,\text{s}^{-1}$, divergence solid, convergence dashed) averaged over the 6 h before MCS initiation. For all columns, the rows show results for the different regions as introduced in Fig. 4. The number of MCS initiations (the composite size) is given in the parentheses. Shown are always the anomalies against a time of day reference state obtained by 12-day low-pass filtering. Dots indicate statistical significance at the 5% level tested by bootstrapping with 5000 iterations.

controls both the TEJ and Sahel rainfall simultaneously. Large-scale SST anomalies and their effect on the planetary-scale tropical circulation are a potential candidate, since they are not only linked to Sahel rainfall changes on interannual and (multi)decadal time scales (Folland et al. 1986; Janicot et al. 1996; Giannini et al. 2003; Bader and Latif 2003), but also affect the TEJ

intensity over India (Abish et al. 2013; Chen and van Loon 1987; Nithya et al. 2017) and over West Africa (Preethi et al. 2015). In ongoing idealized model experiments, we seem to be able to confirm the role of global SST anomalies as said "third variable". By inducing changes in the planetary-scale tropical circulation through anomalous diabatic heating, large-scale

SST anomalies influence both Sahel precipitation and the TEJ largely independently, but in a way that years of higher precipitation are usually accompanied by a stronger TEJ. Thereby, a high statistical connection between the regional TEJ and Sahel rainfall on interannual to multidecadal time scales is possible without any strong underlying interaction.

The second part of this study revisits the role of TEJ-induced upper-level divergence in promoting convection over the Sahel. By analyzing only 17 MCS initiation cases, Besson and Lemaître (2014) concluded that TEJ streaks and associated anomalous upper-level divergence might be favorable for the development of well-organized and persistent MCSs. In contrast, we use a statistical approach with a larger sample size (287 MCS initiation cases) to investigate the synoptic upper-level wind conditions under which MCSs form and find the following:

- In the majority of cases, MCS initiation is not associated with TEJ streaks or any other significant anomalies of the upper-tropospheric wind field
- TEJ streak-related upper-level divergence and/or anomalous TEJ intensity are not correlated with size, lifetime, intensity or movement speed of MCSs

Our analysis does not rule out that there are individual cases in which a pronounced TEJ streak could significantly aid MCS development. Thus, the presented results do not necessarily contradict those of Besson and Lemaître (2014). Because of the much larger sample size, however, it becomes clear that jet streaks on the TEJ do not occur in conjunction with MCSs in most cases, that is, prior to their initiation. Only after an MCS has already formed, may its anticyclonic divergent outflow alter upper-level winds such that the zonal wind field resembles a classic jet streak configuration. Our results therefore cast doubt on the validity of a jet streak–based conceptual framework at very low latitudes and, more generally, question the relevance of synoptic-scale ascent for promoting tropical convection. Thus, our findings are consistent with previous theoretical work which emphasized that balanced dry ascent is weak in the tropics (e.g., Charney 1963; Raymond et al. 2015) and that synoptic-scale vertical motions are typically too weak to play a primary role for convection (e.g., Doswell and Bosart 2001).

In summary, this study challenges the previously proposed hypothesis that the TEJ might play an important role for Sahel rainfall via its control on upper-level divergence. Our multiple statistical analyses show that the regional TEJ intensity over West Africa is only weakly correlated with Sahel rainfall on synoptic to intraseasonal time scales. More importantly, anomalies in convective activity appear to cause changes in the regional TEJ and not the other way around, which suggests a rather passive role for the TEJ. This result is further confirmed by the in-depth analysis of nearly 300 MCSs for which neither their initiation nor their degree of organization is significantly associated with TEJ-induced upper-level divergence or anomalous TEJ intensity.

Some questions, however, remain open due to the limitations of our study. First, by confining our analysis to the satellite era (after 1979) we cannot cover the wet WAM period of the 1950s and 1960s which was characterized by a stronger statistical relationship between rainfall and the TEJ (Fig. 1). Therefore it cannot be ruled out that the more intense TEJ over West Africa might have played a more active role for Sahel rainfall in that period. Another limitation is the use of OLR as a proxy for rainfall. The advantage of using OLR, namely its availability for about four decades in almost gapless, spatially homogeneous datasets, could be partly offset by the disadvantage that the correlation between OLR and rainfall might decrease on subsynoptic spatial and daily or subdaily time scales. For instance, the lowest OLR values associated with an MCS do not necessarily indicate its convective core region, which can lead to several inaccuracies. An additional problem is the coarse temporal (3 h) and spatial resolution (1°), not only of the OLR dataset, but also of the reanalyses. Because the TEJ and possible embedded streaks are mainly synoptic-scale features, we are nonetheless confident that they are reasonably well represented by reanalyses. Therefore, one of our study's focuses, the analysis of the upper-tropospheric flow prior to the formation of MCSs, should not be limited too severely by low resolution. However, it is not possible for us to investigate a potential interaction between the mesoscale flow of an already developed MCS and the synoptic-scale upper-level flow due to the mainly resolution-related limitations of reanalyses.

Moreover, and most importantly, the TEJ could still have an influence on Sahel rainfall via other mechanisms than through affecting upper-level divergence. For instance, the role of the observed planetary-scale waves at the TEJ and their possible interaction with AEWs and synoptic-scale convection was stressed in Nicholson et al. (2007) and Mekonnen and Thorncroft (2016). A further important question is whether not only fluctuations but rather the background mean state of the TEJ influences Sahel rainfall. Yang et al. (2018) showed that AEW activity depends on the background mean flow in the equatorial upper troposphere. A stronger and wider TEJ is associated with favorable equatorial Rossby wave propagation characteristics which promotes AEW activity.

Therefore, further study is needed to understand what determines the TEJ mean state, how it is affected by remote influences and, in particular, how it interacts with Sahel rainfall.

REFERENCES

Abish, B., P. Joseph, and O. M. Johannessen, 2013: Weakening trend of the tropical easterly jet stream of the boreal summer monsoon season 1950–2009. *J. Climate*, **26**, 9408–9414, https://doi.org/10.1175/JCLI-D-13-00440.1.

Alaka, G. J., Jr., and E. D. Maloney, 2012: The influence of the MJO on upstream precursors to African easterly waves. *J. Climate*, **25**, 3219–3236, https://doi.org/10.1175/JCLI-D-11-00232.1.

Bader, J., and M. Latif, 2003: The impact of decadal-scale Indian Ocean sea surface temperature anomalies on Sahelian rainfall and the North Atlantic oscillation. *Geophys. Res. Lett.*, **30**, 2169, https://doi.org/10.1029/2003GL018426.

Besson, L., and Y. Lemaître, 2014: Mesoscale convective systems in relation to African and tropical easterly jets. *Mon. Wea. Rev.*, **142**, 3224–3242, https://doi.org/10.1175/MWR-D-13-00247.1.

Burpee, R. W., 1972: The origin and structure of easterly waves in the lower troposphere of North Africa. *J. Atmos. Sci.*, **29**, 77–90, https://doi.org/10.1175/1520-0469(1972)029<0077:TOASOE>2.0.CO;2.

Carlson, T. N., 1969: Synoptic histories of three African disturbances that developed into Atlantic hurricanes. *Mon. Wea. Rev.*, **97**, 256–276, https://doi.org/10.1175/1520-0493(1969)097<0256:SHOTAD>2.3.CO;2.

Charney, J. G., 1963: A note on large-scale motions in the tropics. *J. Atmos. Sci.*, **20**, 607–609, https://doi.org/10.1175/1520-0469(1963)020<0607:ANOLSM>2.0.CO;2.

Chen, T.-C., and H. van Loon, 1987: Interannual variation of the tropical easterly jet. *Mon. Wea. Rev.*, **115**, 1739–1759, https://doi.org/10.1175/1520-0493(1987)115<1739:IVOTTE>2.0.CO;2.

Couvreux, F., C. Rio, F. Guichard, M. Lothon, G. Canut, D. Bouniol, and A. Gounou, 2012: Initiation of daytime local convection in a semi-arid region analysed with high-resolution simulations and AMMA observations. *Quart. J. Roy. Meteor. Soc.*, **138**, 56–71, https://doi.org/10.1002/qj.903.

Dee, D., and Coauthors, 2011: The ERA-Interim reanalysis: Configuration and performance of the data assimilation system. *Quart. J. Roy. Meteor. Soc.*, **137**, 553–597, https://doi.org/10.1002/qj.828.

Diedhiou, A., S. Janicot, A. Viltard, P. De Felice, and H. Laurent, 1999: Easterly wave regimes and associated convection over West Africa and tropical Atlantic: Results from the NCEP/NCAR and ECMWF reanalyses. *Climate Dyn.*, **15**, 795–822, https://doi.org/10.1007/s003820050316.

Diongue, A., J.-P. LaFore, J.-L. Redelsperger, and R. Roca, 2002: Numerical study of a Sahelian synoptic weather system: Initiation and mature stages of convection and its interactions with the large-scale dynamics. *Quart. J. Roy. Meteor. Soc.*, **128**, 1899–1927, https://doi.org/10.1256/003590002320603467.

Doswell, C. A., III, 1987: The distinction between large-scale and mesoscale contribution to severe convection: A case study example. *Wea. Forecasting*, **2**, 3–16, https://doi.org/10.1175/1520-0434(1987)002<0003:TDBLSA>2.0.CO;2.

——, and L. F. Bosart, 2001: Extratropical synoptic-scale processes and severe convection. *Severe Convective Storms*, Springer, 27–69.

——, H. E. Brooks, and R. A. Maddox, 1996: Flash flood forecasting: An ingredients-based methodology. *Wea. Forecasting*, **11**, 560–581, https://doi.org/10.1175/1520-0434(1996)011<0560:FFFAIB>2.0.CO;2.

Duvel, J. P., 1990: Convection over tropical Africa and the Atlantic Ocean during northern summer. Part II: Modulation by easterly waves. *Mon. Wea. Rev.*, **118**, 1855–1868, https://doi.org/10.1175/1520-0493(1990)118<1855:COTAAT>2.0.CO;2.

EUMETSAT, 2005: Upper level divergence product algorithm description. Tech. Rep. EUM/MET/REP/05/0163, 16 pp.

Fink, A. H., and A. Reiner, 2003: Spatiotemporal variability of the relation between African easterly waves and West African squall lines in 1998 and 1999. *J. Geophys. Res.*, **108**, 4332, https://doi.org/10.1029/2002JD002816.

Folland, C., T. Palmer, and D. Parker, 1986: Sahel rainfall and worldwide sea temperatures, 1901–85. *Nature*, **320**, 602–607, https://doi.org/10.1038/320602a0.

Gelaro, R., and Coauthors, 2017: The Modern-Era Retrospective Analysis for Research and Applications, version 2 (MERRA-2). *J. Climate*, **30**, 5419–5454, https://doi.org/10.1175/JCLI-D-16-0758.1.

Giannini, A., R. Saravanan, and P. Chang, 2003: Oceanic forcing of Sahel rainfall on interannual to interdecadal time scales. *Science*, **302**, 1027–1030, https://doi.org/10.1126/science.1089357.

Grist, J. P., and S. E. Nicholson, 2001: A study of the dynamic factors influencing the rainfall variability in the West African Sahel. *J. Climate*, **14**, 1337–1359, https://doi.org/10.1175/1520-0442(2001)014<1337:ASOTDF>2.0.CO;2.

Huang, X., 2017: A comprehensive Mesoscale Convective System (MSC) dataset, links to files in MatLab and plain text format. PANGAEA, https://doi.org/10.1594/PANGAEA.877914.

Janicot, S., V. Moron, and B. Fontaine, 1996: Sahel droughts and ENSO dynamics. *Geophys. Res. Lett.*, **23**, 515–518, https://doi.org/10.1029/96GL00246.

——, F. Mounier, S. Gervois, B. Sultan, and G. N. Kiladis, 2010: The dynamics of the West African monsoon. Part V: The detection and role of the dominant modes of convectively coupled equatorial Rossby waves. *J. Climate*, **23**, 4005–4024, https://doi.org/10.1175/2010JCLI3221.1.

Kalnay, E., and Coauthors, 1996: The NCEP/NCAR 40-Year Reanalysis Project. *Bull. Amer. Meteor. Soc.*, **77**, 437–471, https://doi.org/10.1175/1520-0477(1996)077<0437:TNYRP>2.0.CO;2.

Kiladis, G. N., and K. M. Weickmann, 1997: Horizontal structure and seasonality of large-scale circulations associated with submonthly tropical convection. *Mon. Wea. Rev.*, **125**, 1997–2013, https://doi.org/10.1175/1520-0493(1997)125<1997:HSASOL>2.0.CO;2.

——, C. D. Thorncroft, and N. M. Hall, 2006: Three-dimensional structure and dynamics of African easterly waves. Part I: Observations. *J. Atmos. Sci.*, **63**, 2212–2230, https://doi.org/10.1175/JAS3741.1.

——, M. C. Wheeler, P. T. Haertel, K. H. Straub, and P. E. Roundy, 2009: Convectively coupled equatorial waves. *Rev. Geophys.*, **47**, RG2003, https://doi.org/10.1029/2008RG000266.

Knapp, K. R., and S. L. Wilkins, 2018: Gridded satellite (GridSat) GOES and CONUS data. *Earth Syst. Sci. Data*, **10**, 1417–1425, https://doi.org/10.5194/essd-10-1417-2018.

Kobayashi, S., and Coauthors, 2015: The JRA-55 reanalysis: General specifications and basic characteristics. *J. Meteor. Soc. Japan Ser. II*, **93**, 5–48, https://doi.org/10.2151/jmsj.2015-001.

Koteswaram, P., 1958: The easterly jet stream in the tropics. *Tellus*, **10**, 43–57, https://doi.org/10.3402/tellusa.v10i1.9220.

Lafore, J. P., and Coauthors, 2017: Deep convection. *Meteorology of Tropical West Africa: The Forecasters' Handbook*, Wiley, 90–129, https://doi.org/10.1002/9781118391297.ch3.

Lebel, T., and A. Ali, 2009: Recent trends in the central and western Sahel rainfall regime (1990–2007). *J. Hydrol.*, **375**, 52–64, https://doi.org/10.1016/j.jhydrol.2008.11.030.

——, A. Diedhiou, and H. Laurent, 2003: Seasonal cycle and interannual variability of the Sahelian rainfall at hydrological scales. *J. Geophys. Res.*, **108**, 8389, https://doi.org/10.1029/2001JD001580.

Lee, H., 2014: Climate algorithm theoretical basis document (C-ATBD): Outgoing Longwave Radiation (OLR)–Daily. Tech. Rep. CDRP-ATBD-0526, NOAA, 46 pp., https://www1.ncdc.noaa.gov/pub/data/sds/cdr/CDRs/Outgoing%20Longwave%20Radiation%20-%20Daily/AlgorithmDescription.pdf.

Maloney, E. D., and J. Shaman, 2008: Intraseasonal variability of the West African monsoon and Atlantic ITCZ. *J. Climate*, **21**, 2898–2918, https://doi.org/10.1175/2007JCLI1999.1.

Mathon, V., and H. Laurent, 2001: Life cycle of Sahelian mesoscale convective cloud systems. *Quart. J. Roy. Meteor. Soc.*, **127**, 377–406, https://doi.org/10.1002/qj.49712757208.

——, ——, and T. Lebel, 2002: Mesoscale convective system rainfall in the Sahel. *J. Appl. Meteor.*, **41**, 1081–1092, https://doi.org/10.1175/1520-0450(2002)041<1081:MCSRIT>2.0.CO;2.

Matsuno, T., 1966: Quasi-geostrophic motions in the equatorial area. *J. Meteor. Soc. Japan Ser. II*, **44**, 25–43, https://doi.org/10.2151/jmsj1965.44.1_25.

Mekonnen, A., and C. D. Thorncroft, 2016: On mechanisms that determine synoptic time scale convection over East Africa. *Int. J. Climatol.*, **36**, 4045–4057, https://doi.org/10.1002/joc.4614.

——, ——, and A. R. Aiyyer, 2006: Analysis of convection and its association with African easterly waves. *J. Climate*, **19**, 5405–5421, https://doi.org/10.1175/JCLI3920.1.

Mounier, F., S. Janicot, and G. N. Kiladis, 2008: The West African monsoon dynamics. Part III: The quasi-biweekly zonal dipole. *J. Climate*, **21**, 1911–1928, https://doi.org/10.1175/2007JCLI1706.1.

Nicholson, S. E., 2009: On the factors modulating the intensity of the tropical rainbelt over West Africa. *Int. J. Climatol.*, **29**, 673–689, https://doi.org/10.1002/joc.1702.

——, 2013: The West African Sahel: A review of recent studies on the rainfall regime and its interannual variability. *ISRN Meteor.*, **2013**, 453521, https://doi.org/10.1155/2013/453521.

——, A. Barcilon, M. Challa, and J. Baum, 2007: Wave activity on the tropical easterly jet. *J. Atmos. Sci.*, **64**, 2756–2763, https://doi.org/10.1175/JAS3946.1.

Nithya, K., M. Manoj, and K. Mohankumar, 2017: Effect of El Niño/La Niña on tropical easterly jet stream during Asian summer monsoon season. *Int. J. Climatol.*, **37**, 4994–5004, https://doi.org/10.1002/joc.5137.

Preethi, B., T. Sabin, J. Adedoyin, and K. Ashok, 2015: Impacts of the ENSO Modoki and other tropical Indo-Pacific climate-drivers on African rainfall. *Sci. Rep.*, **5**, 16653, https://doi.org/10.1038/srep16653.

Rao, P. K., 1952: Probable regions of jet streams in the upper air over India. *Curr. Sci.*, **21** (3), 63–64.

Raymond, D., Ž. Fuchs, S. Gjorgjievska, and S. Sessions, 2015: Balanced dynamics and convection in the tropical troposphere. *J. Adv. Model. Earth Syst.*, **7**, 1093–1116, https://doi.org/10.1002/2015MS000467.

Redelsperger, J.-L., A. Diongue, A. Diedhiou, J.-P. Ceron, M. Diop, J.-F. Gueremy, and J.-P. Lafore, 2002: Multi-scale description of a Sahelian synoptic weather system representative of the West African monsoon. *Quart. J. Roy. Meteor. Soc.*, **128**, 1229–1257, https://doi.org/10.1256/003590002320373274.

Rutan, D. A., S. Kato, D. R. Doelling, F. G. Rose, L. T. Nguyen, T. E. Caldwell, and N. G. Loeb, 2015: CERES synoptic product: Methodology and validation of surface radiant flux. *J. Atmos. Oceanic Technol.*, **32**, 1121–1143, https://doi.org/10.1175/JTECH-D-14-00165.1.

Schulzweida, U., 2019: CDO user guide. Zenodo, https://doi.org/10.5281/zenodo.2558193.

Sultan, B., S. Janicot, and A. Diedhiou, 2003: The West African monsoon dynamics. Part I: Documentation of intraseasonal variability. *J. Climate*, **16**, 3389–3406, https://doi.org/10.1175/1520-0442(2003)016<3389:TWAMDP>2.0.CO;2.

Sylla, M., A. Dell'Aquila, P. Ruti, and F. Giorgi, 2010: Simulation of the intraseasonal and the interannual variability of rainfall over West Africa with RegCM3 during the monsoon period. *Int. J. Climatol.*, **30**, 1865–1883, https://doi.org/10.1002/joc.2029.

Uccellini, L. W., and D. R. Johnson, 1979: The coupling of upper and lower tropospheric jet streaks and implications for the development of severe convective storms. *Mon. Wea. Rev.*, **107**, 682–703, https://doi.org/10.1175/1520-0493(1979)107<0682:TCOUAL>2.0.CO;2.

Van Tuyl, A. H., and J. A. Young, 1982: Numerical simulation of nonlinear jet streak adjustment. *Mon. Wea. Rev.*, **110**, 2038–2054, https://doi.org/10.1175/1520-0493(1982)110<2038:NSONJS>2.0.CO;2.

Wheeler, M., and G. N. Kiladis, 1999: Convectively coupled equatorial waves: Analysis of clouds and temperature in the wavenumber–frequency domain. *J. Atmos. Sci.*, **56**, 374–399, https://doi.org/10.1175/1520-0469(1999)056<0374:CCEWAO>2.0.CO;2.

Yang, G.-Y., B. Hoskins, and J. Slingo, 2007: Convectively coupled equatorial waves. Part I: Horizontal and vertical structures. *J. Atmos. Sci.*, **64**, 3406–3423, https://doi.org/10.1175/JAS4017.1.

——, J. Methven, S. Woolnough, K. Hodges, and B. Hoskins, 2018: Linking African easterly wave activity with equatorial waves and the influence of Rossby waves from the Southern Hemisphere. *J. Atmos. Sci.*, **75**, 1783–1809, https://doi.org/10.1175/JAS-D-17-0184.1.